Materials Chemistry and Physics 133 (2012) 1006–1010

Contents lists available at SciVerse ScienceDirect

Materials Chemistry and Physics

journal homepage: www.elsevier.com/locate/matchemphys

Effect of temperature on the magnetic characteristics of $Ni_{0.5}Co_{0.5}Fe_2O_4$ nanoparticles

K. Maaz [a,c], S. Karim [c], Kyu Joon Lee [b], Myung-Hwa Jung [b], Gil-Ho Kim [a,*]

[a] Department of Electronics and Electrical Engineering and Sungkyunkwan University Advanced Institute of Nanotechnology (SAINT), Sungkyunkwan University, Suwon 440-746, Republic of Korea
[b] Department of Physics, Sogang University, Seoul 121-742, Republic of Korea
[c] Nanomaterials Research Group, Physics Division, PINSTECH, Nilore 45650, Islamabad, Pakistan

ARTICLE INFO

Article history:
Received 10 November 2011
Received in revised form 22 January 2012
Accepted 2 February 2012

Keywords:
Nanostructures
Superparamagnetism
Exchange bias
Ferromagnetism

ABSTRACT

Magnetic nanoparticles of $Ni_{0.5}Co_{0.5}Fe_2O_4$ (size: 18 ± 3 nm) have been synthesized by chemical co-precipitation route. Coercivity (H_C) of the particles shows an increasing behavior with decreasing temperature and observes deviation from the Kneller's law for ferromagnetic nanostructures. Exchange bias effect (H_{ex}) shows an exponential increase with decreasing temperatures followed by a sharp fall below ~5 K. The saturation magnetization (M_s) follows modified Bloch's law in the high temperature range (100–300 K), while below 100 K it shows a decreasing trend with decreasing temperature followed by slow increase in M_s at very low temperatures. Blocking behavior shows a decreasing trend in blocking temperature (T_b) of the system as the applied field in $M(T)$ measurements is increased. The results have been discussed in terms of the variation of anisotropy with temperature, modified spin-wave theory predictions, interparticle interactions, and the presence of spin glass (SG) like phase at the surface of $Ni_{0.5}Co_{0.5}Fe_2O_4$ nanoparticles.

1. Introduction

In single domain nanoparticles the anisotropy determines the spin alignment along the easy axis of magnetization in the system. In such nanoparticle system the thermal fluctuations cause the spins to undergo Brownian-like motion about their easy axes with finite probability that can flip these spins along these axes in the system. The relaxation time (τ) is the average time a spin takes to jump from one easy axis to the other. In the absence of external magnetic field at finite temperature (T) the barrier is the same in either direction and τ is defined by [1]:

$$\tau = \tau_0 \exp\left(\frac{K_{eff}V}{k_B T}\right) \quad (1)$$

where τ_o is a constant called the relaxation or the attempt time of the system, k_B is the Boltzmann constant, K_{eff} is the anisotropy constant, and V is the volume of the nanoparticles. The behavior of a ferromagnet depends strongly on the size of nanoparticles and may differ distinctly for different samples of the same material. It is expected that the experimental measurements sometimes give different results with various equipments of different experimental times (τ_{exp}). Therefore, it is necessary to compare the experimental time with relaxation time of the system, and if $\tau > \tau_{exp}$, then the system is said to be in the blocked or ferromagnetic state. On the other hand, if $\tau < \tau_{exp}$ the spins many flip forth and back during the measurement time and the system behaves like a paramagnet. The average magnetization is given by Langevin function [2]:

$$\langle M \rangle \propto L\left(\frac{\mu H}{k_B T}\right) \quad (2)$$

The behavior is the same as that of a typical paramagnetic system, with no hysteresis but some M_s that is achieved when all the particles are aligned along the field direction. Each particle in this size regime behaves like a huge atom with spin number of 10^3 or 10^4 instead of the order of 1 as in the conventional paramagnets. This phenomenon of the loss of ferromagnetism in small particles is known as superparamagnetism. In Eq. (1) the dependence of τ is strongly on V/T therefore the transition from the stable ferromagnetism to superparamagnetism shifts to smaller sizes when temperature of the system is decreased. The temperature at which such transition occurs (i.e. $\tau = \tau_{exp}$) is called superparamagnetic blocking temperature (T_b) defined by [2]:

$$T_b = \frac{K_{eff}V}{k_B \ln(\tau/\tau_0)} \quad (3)$$

For $T > T_b$ the particles would appear as superparamagnetic while for $T < T_b$ the particles with same sizes will show stable ferromagnetic behavior and are said to be blocked at one of the

* Corresponding author.
E-mail address: ghkim@skku.edu (G.-H. Kim).

0254-0584/$ – see front matter © 2012 Elsevier B.V. All rights reserved.
doi:10.1016/j.matchemphys.2012.02.007

minimum. Such phenomenon in nanoparticles is very important from the application point of view when high or low blocking temperatures are required for their specific applications.

In literature ferrite nanoparticles are reported to be synthesized by a number of techniques [3–6]. In the present work we have used chemical coprecipitation route to synthesize $Ni_{0.5}Co_{0.5}Fe_2O_4$ nanoparticles with sizes of ~18 nm. Their temperature dependent magnetic characterization has been performed in detail from 300 down to 2 K and the results have been explained with reference to the finite size effects, surface spin disorder, and the interparticle interactions in $Ni_{0.5}Co_{0.5}Fe_2O_4$ nanoparticles. This is the first detailed study of this kind for this particular concentration of nickel doped cobalt ferrite nanoparticles.

2. Experimental details

2.1. Materials

The chemical used for synthesis of $Ni_{0.5}Co_{0.5}Fe_2O_4$ nanoparticles include iron chloride, cobalt chloride, nickel chloride, double distilled de-ionized water, sodium hydroxide, and oleic acid.

2.2. Synthesis procedure

Fig. 1 shows the block diagram of coprecipitation process followed for synthesis of $Ni_{0.5}Co_{0.5}Fe_2O_4$ nanoparticles. 25 ml of 0.4 molar (M) iron chloride and 0.2 M cobalt- and nickel-chloride solutions (each of 12.5 ml) were prepared stoichiometrically in double distilled de-ionized water. 25 ml of 3 M sodium hydroxide solution was slowly added to the mixture of above solutions drop-wise and pH of the reaction was constantly monitored. The reactants (combined solution of 75 ml) were vigorously stirred until a pH of ~12 was achieved. A specific amount (2–3 drops for 75 ml solution) of oleic acid was added as the surfactant. The reaction was carried out at ~80 °C under vigorous stirring for 1 h. Since this is an endothermic reaction therefore the heating at 80 °C is required to start the coprecipitation process [3]. After the reaction the product was cooled to room temperature and washed twice with distilled water and ethanol to remove the excess surfactant form the prepared nanoparticles. The sample was centrifuged for 15 min and then dried overnight at 80 °C. The acquired substance was grinded into the fine powders and annealed at 600 °C for 6 hrs to get the desired nanoparticles. Structural analysis of the particles was carried out by X-ray diffraction (XRD) and transmission electron microscopy (TEM). Further details of synthesis procedure for Co- and Ni-ferrite nanoparticles are reported in our previous articles [7,8].

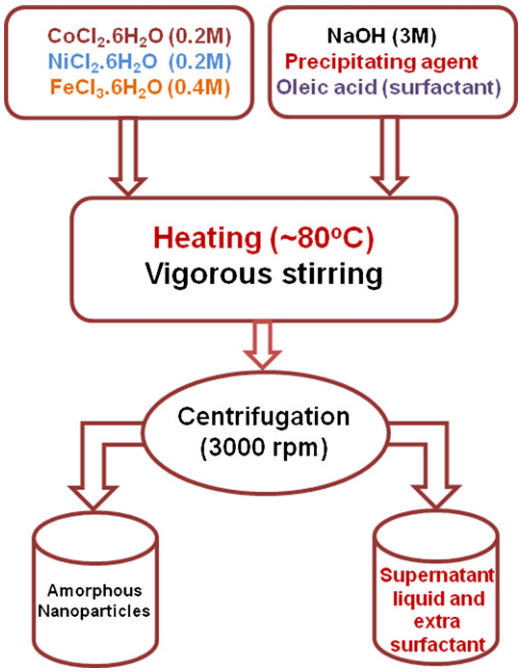

Fig. 1. Schematic diagram of coprecipitation process for synthesis of Ni doped $CoFe_2O_4$ nanoparticles.

3. Results and discussions

Fig. 2(a) shows the XRD pattern of the cubic $Ni_{0.5}Co_{0.5}Fe_2O_4$ nanoparticles according to JCPDF cards. These cards (742081 and 791744) are shown in the inset of XRD figure for the reference purpose. The XRD pattern confirms the polycrystalline Ni-Co ferrite nanoparticles. From the XRD line broadening of the strongest (3 1 1) peak the crystallite size was calculated using Debye-Scherrer equation. TEM analysis shown in Fig. 2(b) confirms the particle size of 18 ± 3 nm. The crystallite size obtained from XRD analysis is 16 nm, which is smaller than the particle size obtained from TEM analysis. We have correlated magnetization data with particle size rather than crystallite size. The average particle-size and size-distribution was analyzed by TEM characterization shown in Fig. 2(b). The size distribution was calculated by finding the frequency of particular size selected in the TEM images and then plotted particle-size versus frequency as shown in the inset histogram of Fig. 2(b). The size-distribution is symmetric and follows the Gaussian distribution with an average size of about 18 nm. From TEM image shown in Fig. 2(b) some particles are seen separated

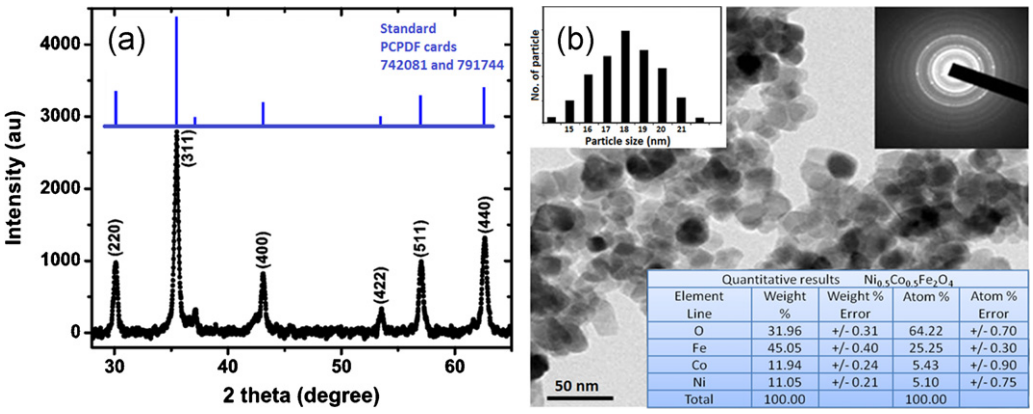

Fig. 2. (a) X-ray diffraction pattern and (b) transmission electron micrograph (TEM) of $Ni_{0.5}Co_{0.5}Fe_2O_4$ nanoparticles. The insets show the SAED and EDS results and the histogram for size distribution in the samples.

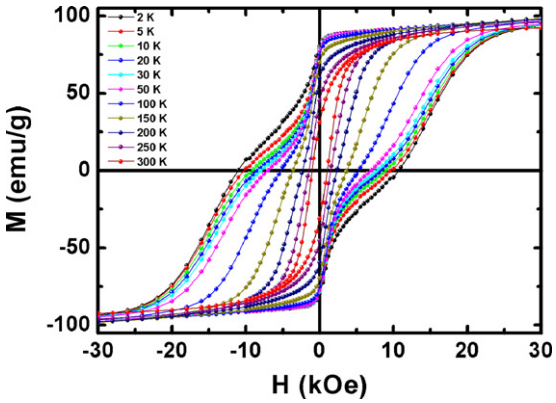

Fig. 3. MH loops of $Ni_{0.5}Co_{0.5}Fe_2O_4$ nanoparticles taken at 2, 5, 10, 20, 30, 50, 100, 150, 200, 250, and 300 K with maximum field of 30 kOe.

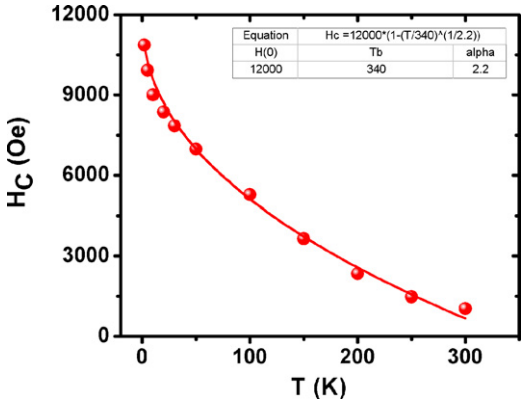

Fig. 4. Temperature depend coercivity of nanoparticles. The red line shows the fit curve according to modified Kneller's law.

from each other however some agglomerated particles are also present in the samples. Possible reason for the agglomeration is the high temperature heat treatment that evaporates the surfactant material and aggregates the nanoparticles with each other. The selected areas electron diffraction (SAED) pattern of the samples shown in the inset of Fig. 2(b) confirms the crystalline nature of nanoparticles while the energy dispersive spectroscopy (EDS) results shown in the inset table indicate the quantitative (weight and atomic percent) presence of various elements constituting the nanoparticles.

Magnetic characterization of $Ni_{0.5}Co_{0.5}Fe_2O_4$ nanoparticles was performed by SQUID magnetometer from 2 to 300 K. Fig. 3 shows the $M(H)$ loops at 2, 10, 30, 100, 15, 200, 250, and 300 K with maximum field of 30 kOe. The hysteresis loops at 2, 5, 10, 20, 30, 50, and 100 K are "bee-waist" type as shown in Fig. 3. If we compare this data with individual Ni- and Co-ferrite $M(H)$ loops reported in our previous articles [7,8] which show normal hysteresis behaviors. We conclude that the two different magnetic phases, i.e. soft Ni-ferrite phase and hard Co-ferrite phase are responsible for the bee-waist type behavior in the samples due to their different coercivities [9,10]. This shows that our nanoparticles are composed of a mixture of two different phases of Ni- and Co-ferrite rather than single homogeneous phase.

The coercivity (H_C) values deducted from the $M(H)$ curves at different temperatures are tabulated in Table 1 and plotted in Fig. 4. It is seen that H_C increases monotonically as T decreases and below ~30 K the increase in H_C becomes very fast. This behavior can be understood by considering the effect of thermal fluctuations of the blocked moments across the anisotropy barriers. For an assembly of non-interacting single domain magnetic nanoparticles with uniaxial anisotropy the H_C in the temperature range

Table 1
Coercivity, exchange bias and saturation magnetization of the nanoparticles at different temperatures.

T (K)	H_C (Oe)	H_{ex} (Oe)	M_S (emu/g)
2	10,864	176	103.55
5	9925	311	103.55
10	9005	187	103.45
20	8366	108	103.45
30	7855	85	103.52
50	6978	54	103.86
100	5275	2	105.01
150	3648	0	105.05
200	2334	0	103.19
250	1477	0	99.82
300	1028	0	95.50

($0–T_B$) can be written in the form of a simple model (Kneller's law) as [11,12]:

$$H_C = H_o\left(1 - \frac{T}{T_B}\right)^{\alpha} \quad (4)$$

where H_o is the zero-temperature coercivity and α is a constant equal to 0.5. In Fig. 4 the red line is the fit curve according to the above relation with modified value of $\alpha \approx 0.455$ smaller than 0.5 used in the above relation (Eq. (4)). The equation with smaller α value is known as the modified Kneller's law. From this curve the zero-temperature coercivity comes out to be ~12 kOe while the coercivity at 2 K is ~10.9 kOe. The deviation of the data from the normal Kneller's law (Eq. (4)) is explained on the basis of core–shell model and the effect of interparticle dipole–dipole magnetic interactions in the samples. It is to be noticed that the samples were annealed at 600 °C at which the surfactant (oleic acid) is expected to be evaporated and the particles are no more coated and expected to be in direct contact with each other. Therefore, the role of interparticle interactions is more likely to be there while performing magnetic characterization of the samples. In case of core–shell nanoparticles the core spins are ferromagnetically or ferrimagnetically aligned while the shell spins are tilted or in the randomized state because of the broken exchange bonds at the surface of the particles. This gives the shell-spins to freeze into their random states at reduced temperatures and giving no good response to the external field. In case of smaller nanoparticles (i.e. 18 nm in our case) this effect becomes more pronounced as compared to larger particles. This resultantly weakens the temperature response of H_C in this case. However, the dominant role of deviating from the Kneller's law is the interparticle interactions in our case. If we notice in Fig. 2(b) it is seen that the nanoparticles are aggregated, which can lead to the strong interparticle interactions among the nanoparticles while taking the magnetic data of the samples. In this case, apart from the anisotropy energy (E_A) of individual nanoparticle, there is some contribution from orientational magnetic interaction energy towards the total anisotropy energy of the system that can lead the spins to flip across the anisotropy energy barrier [13]. Thus the interparticle interactions play a dominant role in the samples and cause the deviation from the normal Kneller's law in these $Ni_{0.5}Co_{0.5}Fe_2O_4$ nanoparticles.

In the exchange bias studies the nanoparticles are cooled from room temperature ($T < T_c$) to a lower temperature ($T < T_N$) in the presence of some field (FC measurements) and then hysteresis loops are taken. The consequent horizontal shift in FC–$M(H)$ loops is termed as the exchange given by $H_{ex} = (H_{C2} - H_{C1})/2$ where H_{C1} and H_{C2} are the absolute values of positive and the negative coercivities. H_{ex} is resulting in a bi-layer system (core–shell structure in our case) where an antiferromagnetic material with strong anisotropy

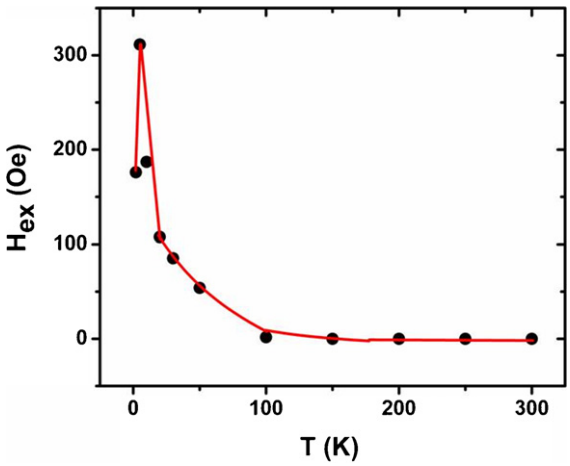

Fig. 5. Dependence of exchange field on temperature for $Ni_{0.5}Co_{0.5}Fe_2O_4$ nanoparticles. The pronounced increase in H_{ex} is evident in the temperature range 5–100 K.

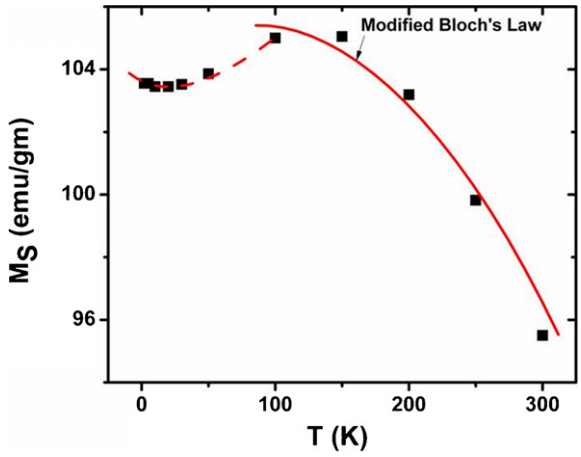

Fig. 6. Saturation magnetization as a function of temperature for $Ni_{0.5}Co_{0.5}Fe_2O_4$ nanoparticles. The red line is the fit curve according to modified Bloch's law for saturation magnetization of the nanoparticles.

(shell) is deposited on the top of a low anisotropy ferromagnetic material (core). The values of H_{ex} are calculated using above relation from 2 to 300 K under a cooling field of 5 kOe and then plotted as function of temperature as shown in Fig. 5 and tabulated in Table 1. It is seen that above 100 K H_{ex} is negligible, while below 100 K H_{ex} increases with decreasing temperature up to ~5 K, and finally a sharp fall is observed below this temperature. We anticipate that H_{ex} arises due to the interaction between the core and surface spins (shell) at the core–shell interface. In this case the core spins are aligned ferrimagnetically while the situation at the surface may be quite complex. In general the atomic coordination number at the surface of nanoparticles is different from that of the core and this variation causes disturbance in the crystal field that destabilizes the magnetic order at the shell region. The spin alignments can take a multiplicity of forms [14] with several different ground states and resulting the shell spins to act in the spin glass (SG) like manner [15–17]. Therefore the particles behave like the core–shell system similar to the metal–metal oxide nanoparticles with oxide shell covering the metallic core of the nanoparticles [18]. The core shell interaction at the interface gives rise to the phenomenon of exchange bias effect in this system. The observed temperature dependence of H_{ex} can be explained on the basis of phenomenological model where H_{ex} has been estimated to vary as [18]:

$$H_{ex} = \frac{E_{int}}{M_{FM} t_{FM}} \tag{5}$$

where E_{int} is the interfacial exchange energy, t_{FM} is the thickness of ferro- or ferri-magnetic core and M_{FM} is magnetization. Now to interpret our data (Fig. 5) we assume that the decrease of H_{ex} above 100 K may be the thermal fluctuations that destabilize the core–shell interface spin interactions thereby weakening this effect at higher temperatures. Below 100 K the anisotropy of the system increases as a result of thermal suppression in the system. The enhancement of the anisotropy with decreasing temperature can reinforce the spin interactions at the core–shell interface thereby increasing H_{ex} below 100 K. At very low temperatures, below ~5 K there is an increasing trend in magnetization of the samples (see Fig. 6) and hence by the virtue of Eq. (5) H_{ex} is going to decrease, provided the interfacial energy of the system does not vary. The apparent increase in magnetization of the system at lower temperatures shown in Fig. 6 could be the result of interparticle dipole–ipole magnetic interactions in the samples that play dominant role at low temperatures (below 5 K) when the thermal energy is suppressed. In Fig. 6 it is evident that M_S increases with decreasing temperature in accordance with Bloch's law for ferromagnetic materials. These values at different temperatures are tabulated in Table 1. For a bulk ferromagnetic/ferrimagnetic system the saturation magnetization below the Curie temperature follows the Bloch's law of the form [19]:

$$M(T) = M(0)\left[1 - \left(\frac{T}{T_o}\right)^{\alpha}\right] \tag{6}$$

where $(1/T_o)^{\alpha}$ is called the Bloch constant that depends on the structure of the material. $M(T)$ is the temperature-dependent magnetization and α is the Bloch's exponent with a value of 3/2. This law is generally valid for bulk materials in the high temperature range. However, at the nanoscale due the finite size effects the thermal dependence of magnetization deviates from Bloch's law as the magnons with wavelength larger than the particle dimensions cannot be excited and a threshold of thermal energy is required to generate the spin waves in case of nanoparticles. Thus for nanoparticles the spin wave structure is modified in the form of a power law (T^{α}) with Bloch's exponent larger than its bulk value of 3/2, which is called the modified Bloch's law [20,21]. The value of α in the modified Bloch's law has been experimentally determined by Auino et al. [22]. They have found that for large size $CuFe_2O_4$ nanoparticles the value of α is 3/2 whereas for smaller nanoparticles this value is close to 2. In our system (Fig. 6) this model is valid only in high temperature range (300–100 K) while below 100 K there is a decreasing trend in saturation magnetization of the system and the experimental data show a deviation from this law. Thus the modified spin-wave spectrum is applicable to these nanoparticles in the temperature range 100–300 K. However, at low temperatures (<100 K) the decrease in magnetization may be attributed to the SG like layer at the surface of nanoparticles that prevents the core spins to align along the field direction when the external field is applied. In Fig. 6 at very low temperatures <5 K there is slight increasing trend in magnetization that can be attributed to dipole–dipole interactions in the sample as discussed earlier.

Finally, to explore the effect of external field on blocking temperature (T_b) various $M(T)$ curves have been taken at different applied fields. Fig. 7 shows T_b as a function of the field with inset of the figure shows FC and ZFC curves for one of the representative sample. It is important to mention that T_b is not the true superparamagnetic blocking temperature of the nanoparticles in our case; however it is proportional to the true blocking temperature of the system. It is seen in the inset of Fig. 7 that the ZFC peak is broad. The broad peak is due to the large size distribution or due to interparticle dipole–dipole interactions in the samples. Close examination of Fig. 2(b) confirms the possibility of dipole–dipole interactions

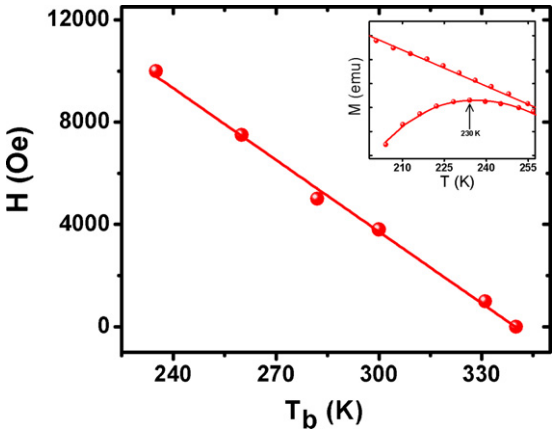

Fig. 7. Blocking temperature as a function of applied field. The inset of the figure shows an $M(T)$ curve for one of the representative sample.

as there are many aggregated particles present in the images. In this study it is seen in Fig. 7 that the nanoparticles are in the blocked ferromagnetic state (non-zero coercivity) at 300 K when H is very small. The non-zero coercivity is either due to the presence of micro-scale particles or due to the large size-distribution in the samples. The first possibility is excluded as there is no evidence of micro-scale particles in TEM image shown in Fig. 2(b). Therefore, the only possibility of non-zero coercivity (blocked particles) at room temperature is due to the size-distribution in the samples. However, as discussed earlier, T_b is not the true superparamagnetic blocking temperature of the system where the zero coercivity is achieved in the samples. Furthermore, it is seen that as the applied field (H) is increased T_b is shifted towards the lower values which is in agreement with previous reports [23,24]. This shows that as the applied field is increased the anisotropy energy barrier is suppressed by an amount (μH) and the spin can easily flip from one energy minimum to the other along the field direction and becomes parallel to the applied field. In this case the anisotropy energy is dominated by the thermal energy that lowers the blocking temperature of the system. The real superparamagnetic blocking temperature of the system can be obtained by extrapolating the H to zero where T_b is ~350 K, which indicates the blocking of the system with $H = 0$. Thus above this temperature the nanoparticles are expected to behave in the superparamagnetic unblocked state. It is worthy to mention that T_b for 18 nm particles has not been reported in the literature so far; however, it is important to know that the interparticle interactions usually increase the overall anisotropy of the samples. This results in the increase of superparamagnetic blocking temperature of the system [13]. If we extrapolate our data to very low field ($H < 100$ Oe) in Fig. 7 we may not be able to observe the superparamagnetic behavior of the samples and all the nanoparticles would be in the blocked ferromagnetic state at room temperature. This might be due to the minute interactions which take place among the nanoparticles at low magnetic field.

4. Conclusion

In this article we have presented synthesis of $Ni_{0.5}Co_{0.5}Fe_2O_4$ nanoparticles of sizes 18 ± 3 nm. Coercivity of the samples showed an increasing behavior with decreasing temperature that has been attributed to the enhanced anisotropy and interparticle interactions at lower temperatures. H_{ex} showed an exponential increase <100 K followed by a sharp fall at ~5 K that has been attributed to the enhanced anisotropy at reduced temperatures and to interparticle interactions in the samples. The saturation magnetization followed the modified Bloch's law is based on the modified spin-wave spectrum that arises as a result of finite size effects. The blocking temperature was found shift to lower values as the external field was increased that has been attributed to the suppression of anisotropy energy as compared to thermal energy that favors the particles to behave in the unblocked state.

Acknowledgment

This research was supported by World Class University program funded by the Ministry of Education, Science and Technology through the National Research Foundation of Korea (R32-10204).

References

[1] L. Neel, Ann. Geophys. (C.N.R.S.) 5 (1949) 99.
[2] A. Aharoni, Introduction to the Theory of Ferromagnetism, Clarendon Press, Oxford, 1996.
[3] H. Yamamoto, Y. Nissato, IEEE Trans. Magn. 33 (5) (2002) 3488.
[4] F. Li, J. Liu, D.G. Evans, X. Duan, Chem. Mater. 16 (2004) 1597.
[5] B.S. Randhawa, H.S. Dosanjh, M. Kaur, Indian J. Eng. Mater. Sci. 12 (2005) 151.
[6] D. Carta, M.F. Casula, A. Falqui, D. Loche, G. Mountjoy, C. Sangregorio, A. Corrias, J. Phys. Chem. C 113 (2009) 8606.
[7] K. Maaz, A. Mumtaz, S.K. Hasanain, A. Ceylan, J. Magn. Magn. Mater. 308 (2007) 289.
[8] K. Maaz, S. Karim, A. Mumtaz, S.K. Hasanain, J. Liu, J.L. Duan, J. Magn. Magn. Mater. 321 (2009) 1838.
[9] Q. Fang, W. Zhong, Z. Jin, Y. Du, J. Appl. Phys. 85 (1999) 1667.
[10] D.M.S. Esquivel, E. Wajnberg, G.R. Cernicchiaro, O.C. Alves, J. Magn. Magn. Mater. 278 (2004) 117.
[11] E.F. Kneller, F.E. Luborsky, J. Appl. Phys. 34 (1963) 656.
[12] X. Batlle, M. Garcia del Muro, J. Tejada, H. Pfeiffer, P. Goand, E. Sinn, J. Appl. Phys. 74 (1993) 3333.
[13] Y. Zhang, Y. Liu, C. Fei, Z. Yang, Z. Lu, R. Xiong, D. Yin, J. Shi, J. Appl. Phys. 108 (2010) 084312.
[14] R.H. Kodama, J. Magn. Magn. Mater. 200 (1999) 359.
[15] J. Nogues, Ivan K. Schuller, J. Magn. Magn. Mater. 192 (1999) 203.
[16] J. Nogues, J. Sort, V. Langlias, V. Skumryev, S. Suriñach, J.S. Muñoz, M.D. Baró, Phys. Rep. 422 (3) (2005) 65.
[17] R.H. Kodama, A.E. Berkowitz, Phys. Rev. Lett. 77 (1996) 394.
[18] R.K. Zheng, G.H. Wen, K.K. Fung, X.X. Zhang, J. Appl. Phys. 95 (2004) 5244.
[19] F. Bloch, Z. Phys. 61 (1931) 206.
[20] S. Mørup, Europhys. Lett. 77 (2007) 27003.
[21] K. Mandal, P. Subarna Mitra, Anil Kumar, Europhys. Lett. 75 (4) (2006) 618.
[22] A. Auino, M.H. Sousa, H.R. Rechenbrg, G.F. Goya, F.A. Tourinho, J. Depeyrot, J. Met. Nanocryst. Mater. 20–21 (2004) 694.
[23] B. Martinez, X. Obradors, Li Balcells, A. Rouanet, C. Monty, Phys. Rev. Lett. 80 (1998) 181.
[24] D. Peddis, C. Cannas, A. Musinu, G. Piccaluga, J. Phys. Chem. C 112 (2008) 5141.